


Cite this: *RSC Adv.*, 2020, 10, 27137

# Effect of C-terminus amidation of A $\beta$ <sub>39–42</sub> fragment derived peptides as potential inhibitors of A $\beta$ aggregation†

Akshay Kapadia,<sup>‡a</sup> Aesan Patel,<sup>‡a</sup> Krishna K. Sharma,<sup>a</sup> Indresh Kumar Maurya,<sup>b</sup> Varinder Singh,<sup>c</sup> Madhu Khullar<sup>c</sup> and Rahul Jain<sup>id</sup> <sup>\*a</sup>

The C-terminus fragment (Val-Val-Ile-Ala) of amyloid- $\beta$  is reported to inhibit the aggregation of the parent peptide. In an attempt to investigate the effect of sequential amino-acid scan and C-terminus amidation on the biological profile of the lead sequence, a series of tetrapeptides were synthesized using MW-SPPS. Peptide D-Phe-Val-Ile-Ala-NH<sub>2</sub> (**12c**) exhibited high protection against  $\beta$ -amyloid-mediated-neurotoxicity by inhibiting A $\beta$  aggregation in the MTT cell viability and ThT-fluorescence assay. Circular dichroism studies illustrate the inability of A $\beta$ <sub>42</sub> to form  $\beta$ -sheet in the presence of **12c**, further confirmed by the absence of A $\beta$ <sub>42</sub> fibrils in electron microscopy experiments. The peptide exhibits enhanced BBB permeation, no cytotoxicity along with prolonged proteolytic stability. *In silico* studies show that the peptide interacts with the key amino acids in A $\beta$ , which potentiate its fibrillation, thereby arresting aggregation propensity. This structural class of designed scaffolds provides impetus towards the rational development of peptide-based-therapeutics for Alzheimer's disease (AD).

Received 31st May 2020

Accepted 10th July 2020

DOI: 10.1039/d0ra04788k

rsc.li/rsc-advances

First reported by Alois Alzheimer in 1906, Alzheimer's Disease (AD) is a progressive, neurodegenerative disorder with an irreversible decline in memory and cognition.<sup>1</sup> It is commonly seen in elderly populations and is marked by two major histopathological hallmarks, amyloid- $\beta$  (A $\beta$ ) plaques and neurofibrillary tangles (NFT).<sup>2</sup> The number of patients suffering from AD has been increasing at an alarming rate. It is estimated that around 60 million patients will be suffering from AD by the end of 2020 and half of this patient population would require the care equivalent to that of a nursing home.<sup>3</sup> Even after a century of its discovery, there has been no treatment that targets the pathophysiology of AD.<sup>4</sup> The current treatment regimen includes acetylcholine-esterase inhibitors (AChEI) comprising of donepezil, rivastigmine and galantamine as well as *N*-methyl-D-aspartate (NMDA)-receptor antagonist, memantine. These provide only symptomatic relief to the patient. Most of the therapeutics that are currently being tested in clinical trials

couldn't proceed beyond phase II and phase III clinical trials due to lower efficacy in elderly patients, multiple side effects and limitations in their pharmacokinetic and pharmacodynamic profiles.<sup>5–9</sup> This has created challenges on the societal and economic upfront.

Literature analysis reveals that the soluble oligomeric A $\beta$  species is the culprit for neurotoxicity. It interrupts normal physiological functioning of the human brain. The central hydrophobic fragment A $\beta$ <sub>16–22</sub> (KLVFFAE) and the C-terminus region fragment A $\beta$ <sub>31–42</sub> (IIGLMVGGVVIA) are responsible for controlling the aggregation kinetics of the monomeric species, wherein the later still remains relatively less explored.<sup>8,9</sup> Our group is focused on development of peptidomimetic analogues for preventing A $\beta$  aggregation. Studies on a complete peptide scan on the C-terminus region regions has already been published previously.<sup>10–12</sup> In an attempt to enhance the biological efficacy of the previously designed scaffolds,<sup>12</sup> we rationalized the use of sequential amino acid scan by modifying/replacing individual residues, as well as amide protection of the C-terminus on the lead tetrapeptide sequence (Val-Val-Ile-Ala) to enhance the proteolytic stability of the peptides.

C-terminus amidated peptides were synthesized by microwave-assisted Fmoc-solid phase peptide synthesis protocol. Scheme 1 shows the general route for the synthesis of peptides employing Rink amide resin (detailed methodology is mentioned in the ESI, Section 1†). These peptides were characterized using by analytical HPLC, <sup>1</sup>H and <sup>13</sup>C NMR, APCI/ESI-MS and HRMS.

<sup>a</sup>Department of Medicinal Chemistry, National Institute of Pharmaceutical Education and Research, Sector 67, S. A. S Nagar, Punjab 160 062, India. E-mail: rahuljain@niper.ac.in; Tel: +91-172-2292024

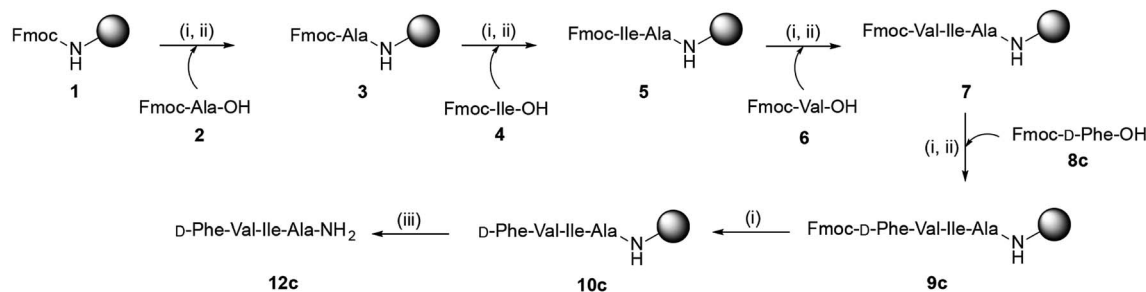
<sup>b</sup>Department of Microbial Biotechnology, Punjab University, Sector 25, Chandigarh, Punjab 160 014, India

<sup>c</sup>Post Graduate Institute of Medical Education and Research, Sector 11, Chandigarh, Punjab, 160 014, India

† Electronic supplementary information (ESI) available: Structural characterization data, representative NMR, HPLC chromatograms and HRMS spectra, detailed experimental procedure, figures and tables. See DOI: 10.1039/d0ra04788k

‡ Equal contribution.





**Scheme 1** Synthesis of tetrapeptide **12c** using MW-assisted Fmoc-solid phase peptide synthesis protocol employing Rink amide resin. Reaction conditions: (i) 20% piperidine in DMF (7 mL), MW (40 W), 60 °C, 2 cycles – 1.5 & 3 min; (ii) **2**, **4**, **6**, **8** (4 equiv.), TBTU (4 equiv.), HoBt (4 equiv.), DIPEA (5 equiv.), DMF (3.5 mL), MW (40 W), 60 °C, 13.5 min; (iii) TFA : TIPS : H<sub>2</sub>O (95 : 2.5 : 2.5), rt, 2.5 h; reaction monitoring was done by: UV measurement: Fmoc deprotection-dibenzofulvene adduct, Kaiser test: 1° amines; acetaldehyde test: 2° amines.

Aggregation of A $\beta$ <sub>42</sub> results in accumulation of toxic species, which interact with neurons and hinder their functioning, leading to loss of memory and cognition. Inhibiting the process of A $\beta$ <sub>42</sub> aggregation would alleviate the neurotoxicity imparted in PC-12 cells; this was evaluated by MTT cell viability assay.<sup>13</sup> Viability of untreated cells is considered 100%. Upon treatment with 2  $\mu$ M of A $\beta$ <sub>42</sub>, only 74% cells were found to be viable. Out of the total tested peptides, seven tetrapeptides **12a**, **12c**, **12f**, **13e**, **14b**, **15b** and **15f** showed complete inhibition of A $\beta$ <sub>42</sub>-induced toxicity by restoring the cell viability to 100%, at respective concentrations. Results for cell viability assay along with Thioflavin-T fluorescence assay for all the synthesized tetrapeptides has been summarized in Table 1.

The quantitative evaluation of  $\beta$ -sheet structures within the amyloid fibrils is accessed by the fluorescence of the Thioflavin-T dye.<sup>14</sup> Inhibiting amyloid fibrillation would reduce or eliminate such an enhancement in fluorescence. This concept is utilized to evaluate compounds that would prevent A $\beta$  from aggregating.<sup>15–17</sup> ThT fluorescence in the presence of A $\beta$ <sub>42</sub> alone was considered 100% and % relative fluorescence unit (% RFU) values were calculated for A $\beta$ <sub>42</sub> co-incubated with the respective inhibitor peptides. ThT incubated alone, exhibited % RFU of nearly 53.3% as compared to control solution without dye. Complete data of % inhibition of A $\beta$ <sub>42</sub> by the test peptides has been summarized in Table 1.

The lead peptide **11** Val-Val-Ile-Ala-OH, was observed to mitigate the A $\beta$ <sub>42</sub> aggregation by 33.9, 60.6 and 66.2% at 2  $\mu$ M, 4  $\mu$ M and 10  $\mu$ M concentrations whereas peptide **11a** shows increased activity at 2  $\mu$ M but slightly less activity at higher dose concentrations in both cell viability and ThT-fluorescence assays.<sup>17</sup> Out of all the tested peptides, peptides **12c** and **13e** showed minimal enhancement in ThT fluorescence when co-incubated with equimolar concentrations of A $\beta$ <sub>42</sub>. Peptides **12f** and **12g** showed >90% activity at five-fold excess dose concentrations. A comparative bar graph representation for the four most active peptides **12c**, **12f**, **12g** and **13e** has been depicted in Fig. 1A. To understand the % RFU values indicating the relative fluorescence of ThT and % inhibition exhibited by the most active test peptides **12c**, **12f**, **12g** and **13e**, values have been summarized in ESI, Tables S1 and S2.† The observed RFU was close to that of the control wells where the dye incubated alone.

Negligible increment of ThT fluorescence when the test peptides are co-incubated with A $\beta$ <sub>42</sub> peptide clearly indicates the inhibition of fibrillation. It also provides further support to the inhibition of A $\beta$ <sub>42</sub>-induced neuronal toxicity as studied in the MTT assay. The % inhibition of A $\beta$ <sub>42</sub> aggregation as depicted by the ThT fluorescence assay is in accordance with the % cell viability data obtained by the MTT assay. Exact correlation cannot be established between the two because of the differential behavior of A $\beta$ <sub>42</sub> in the presence of a cellular environment as well as the treatment/incubation time for both the experiments.

Peptides **12c** and **12f** that exhibited >98% cell viability at the lowest tested concentration of 2  $\mu$ M were then evaluated at lower dose concentrations of 1.0  $\mu$ M, 0.5  $\mu$ M and 0.1  $\mu$ M, against 2  $\mu$ M of A $\beta$ <sub>42</sub> maintaining the ratios of 1 : 2, 1 : 4 and 1 : 20 (test peptide : A $\beta$ <sub>42</sub>), respectively. The graphical plot of dose dependent modulation of A $\beta$ <sub>42</sub> aggregation-induced-neurotoxicity in PC-12 cells is depicted in Fig. 1C. Peptide **12c** exhibited 78% inhibition of A $\beta$ <sub>42</sub> even at a lowest tested dose of 0.1  $\mu$ M. A graphical representation of the % decrease in RFU has been depicted in Fig. 1B and dose dependent % inhibition of A $\beta$ <sub>42</sub> aggregation has been depicted in Fig. 1D. Excellent activities were exhibited when the test peptide is present in equimolar concentrations of A $\beta$ <sub>42</sub>, indicating 1 : 1 inhibition of the parent peptide.

Upon the basis of careful analysis of data reported herewith and results published earlier,<sup>10–12</sup> a correlation between the amino acid residues within the tetrapeptide sequence and the exhibited activity was established. Replacement of the first residue, Val<sub>39</sub> with hydrophobic residues (Phe and D-Phe) exhibited >90% inhibition. The replacement of Val<sub>40</sub> with hydrophobic (Phe, D-Ile) or conformationally restricted amino acids (Pro, Aib) slightly enhanced the potency of the peptide. This holds true even in dual substitution at Val<sub>39</sub> and Val<sub>40</sub>. Any replacement or modification yielded less active derivatives, indicating Ile<sub>41</sub> is critical for activity. Small analogous amino acid is preferred at the Ala<sub>42</sub> for retaining the activity. Amidation of the C-terminus results in enhancement of inhibition potential for some peptides. In some cases, a decrease in activity is also observed. A summary of the SAR is shown in Fig. 2. Understanding the sequential positioning of these residues



**Table 1** % cell viability against A $\beta$ <sub>42</sub> aggregation-induced-neurotoxicity and % inhibition of A $\beta$ <sub>42</sub> aggregation exhibited by the test peptides

No.	Test peptide sequence <sup>a</sup>	MTT cell viability assay			ThT-fluorescence assay		
		Test peptide concentration range (A $\beta$ <sub>42</sub> : test peptide)					
		10 $\mu$ M (1 : 5)	4 $\mu$ M (1 : 2)	2 $\mu$ M (1 : 1)	10 $\mu$ M (1 : 5)	4 $\mu$ M (1 : 2)	2 $\mu$ M (1 : 1)
		% viable cells <sup>b</sup>			% inhibition <sup>d</sup>		
11	Val-Val-Ile-Ala-OH (lead)	93.6	90.5	78.9	66.2	60.6	33.9
11a	Val-Val-Ile-Ala-NH <sub>2</sub>	82.2	89.3	86.4	52.1	52.7	58.8
12a	D-Val-Val-Ile-Ala-NH <sub>2</sub>	81.6	100.0	94.8	82.1	83.5	64.7
12b	Phe-Val-Ile-Ala-NH <sub>2</sub>	92.1	95.7	96.2	77.6	66.2	51.9
12c	D-Phe-Val-Ile-Ala-NH <sub>2</sub>	100.0	95.2	98.4	100.0	100.0	100.0
12d	D-Pro-Val-Ile-Ala-NH <sub>2</sub>	92.0	83.5	82.8	39.8	52.9	60.8
12e	Nva-Val-Ile-Ala-NH <sub>2</sub>	83.4	86.1	74.1	70.3	51.9	77.2
12f	Aib-Val-Ile-Ala-NH <sub>2</sub>	61.3	95.1	100.0	93.8	66.0	64.5
12g	Gly-Val-Ile-Ala-NH <sub>2</sub>	75.4	94.3	92.1	98.1	64.5	84.4
13a	Val-D-Val-Ile-Ala-NH <sub>2</sub>	87.6	75.2	74.7	15.7	46.5	89.3
13b	Val-D-Ile-Ile-Ala-NH <sub>2</sub>	94.6	92.8	90.3	49.4	35.1	65.6
13c	Val-Pro-Ile-Ala-NH <sub>2</sub>	83.1	96.0	93.0	18.5	16.3	31.8
13d	Val-Aib-Ile-Ala-NH <sub>2</sub>	100.0	93.0	75.1	45.3	50.0	52.1
13e	Val-Phe-Ile-Ala-NH <sub>2</sub>	93.3	100.0	79.3	57.2	61.7	100.0
13f	Val-D-Phe-Ile-Ala-NH <sub>2</sub>	99.7	92.9	94.2	62.5	66.2	75.8
14a	Val-Val-D-Ile-Ala-NH <sub>2</sub>	69.6	76.5	79.7	21.8	25.3	49.6
14b	Val-Val-Leu-Ala-NH <sub>2</sub>	86.3	100.0	83.8	0.0	16.5	42.2
15a	Val-Val-Ile-D-Ala-NH <sub>2</sub>	93.8	80.2	83.3	23.2	14.6	68.6
15b	Val-Val-Ile-Aib-NH <sub>2</sub>	99.1	100.0	71.9	35.1	42.0	24.9
15c	Val-Val-Ile-Gly-NH <sub>2</sub>	90.5	88.5	80.7	5.4	31.8	62.7
15d	Val-Val-Ile-Val-NH <sub>2</sub>	71.7	75.4	64.5	11.0	6.9	0.0
15e	Val-Val-Ile-Leu-NH <sub>2</sub>	70.6	71.7	89.4	31.2	30.0	18.7
15f	Val-Val-Ile-Ile-NH <sub>2</sub>	100.0	97.0	78.6	48.2	0.0	0.0
16a	Pro-Pro-Ile-Ala-NH <sub>2</sub>	77.7	60.7	74.6	14.2	18.3	24.7
A $\beta$ <sub>42</sub>			74.05				
Control <sup>c</sup>			100.0				

<sup>a</sup> Amino acid residue modified within the tetrapeptide sequence is indicated in bold. <sup>b</sup> Cell viability studies were performed using MTT cell viability assay against PC-12 cells. <sup>c</sup> The percentage of untreated cells was considered 100% (positive control); percentage cell viability was calculated for the cells incubated along with A $\beta$ <sub>42</sub> (2  $\mu$ M) in absence (negative control) and presence of the test peptides in respective dose concentrations for 6 h. % of viable cells was calculated by the formula as  $100 \times [\text{A}\beta_{42} + \text{test peptide OD}_{570} - \text{A}\beta \text{ OD}_{570} / \text{control OD}_{570} - \text{A}\beta \text{ OD}_{570}]$ . In a subset of triplicate wells, standard deviation values ranged 1.81–4.72. <sup>d</sup> Inhibition of A $\beta$ <sub>42</sub> aggregation was calculated by Thioflavin-T fluorescence assay. % relative fluorescence units (% RFU) exhibited by A $\beta$  fibrils were considered as 100%. ThT dye incubated alone was considered as control and % RFU units were computed when A $\beta$ <sub>42</sub> was co-incubated with the test peptides for 24 h ( $\lambda_{\text{ex}}$  440 nm,  $\lambda_{\text{em}}$  485 nm). % inhibition of ThT fluorescence was calculated by using the formula:  $100 \times [100 - (\text{A}\beta_{42} + \text{test peptide RFU}_{485} - \text{control RFU}_{485} / \text{A}\beta_{42} \text{ RFU}_{485} - \text{control RFU}_{485})]$ . In a subset of triplicate wells, SD values ranged 1.22–4.83. Data for both the experiments was recorded for triplicate samples and the readings were averaged (<5% variation).

would help us further develop derivatives with enhanced potency to inhibit A $\beta$ <sub>42</sub> aggregation.

It is reported that there are two species of A $\beta$  *i.e.* A $\beta$ <sub>40</sub> and A $\beta$ <sub>42</sub>, present in the diseased brain.<sup>18–20</sup> Evaluating the inhibitory activities of the test compounds on the aggregation of both the species would be of biological significance.<sup>21</sup> Therefore, inhibitory potential of peptide 12c was evaluated on A $\beta$ <sub>40</sub>. The relative increase in the ThT fluorescence when A $\beta$ <sub>40</sub> was incubated alone for 24 h was very less or similar to that of the control wells containing ThT (Fig. 3A). Further testing for 48 h and 72 h, respectively yielded no substantial results (ESI, Table S3†).

The minimal increase in fluorescence could be attributed to the slower nucleation rate and longer lag phase in the kinetics of A $\beta$ <sub>40</sub> fibril formation in comparison to A $\beta$ <sub>42</sub>.<sup>22–24</sup> Also, A $\beta$ <sub>40</sub> is relatively less neurotoxic and its aggregation propensity enhances in the presence of A $\beta$ <sub>42</sub>, although the former is present in a ten-fold higher concentration. Thus, evaluation of

the inhibitory activity of test peptide 12c on the mixtures of A $\beta$ <sub>40</sub> : A $\beta$ <sub>42</sub> in the ratio of 10 : 1 was performed. On incubation of a mixture of 5  $\mu$ M of A $\beta$ <sub>40</sub> and 0.5  $\mu$ M of A $\beta$ <sub>42</sub> (ratio of 10 : 1) the % relative increase in ThT fluorescence was comparatively higher than when A $\beta$ <sub>40</sub> was incubated alone (Fig. 3B). When compared to that of A $\beta$ <sub>42</sub> incubated alone as analyzed in the previous experiments, the fluorescence intensities were less. This gave us a clear indication that the aggregation propensity of A $\beta$ <sub>40</sub> is amplified in the presence of 0.1 equimolar A $\beta$ <sub>42</sub>. On co-incubation of the test peptide 12c with the 5  $\mu$ M mixture of A $\beta$ <sub>40</sub> : A $\beta$ <sub>42</sub> in the ratio of 10 : 1, substantial decrease in the fluorescence levels were observed (ESI, Table S4†).

As a prophylactic measurement, the potential ability of the test peptides to deform the aggregated A $\beta$ <sub>42</sub> was investigated.<sup>25,26</sup> Monomeric A $\beta$ <sub>42</sub> was pre-incubated for a period of 24 h and fluorescence was measured. As anticipated, there was a marked increase in the fluorescence due the fibril state of



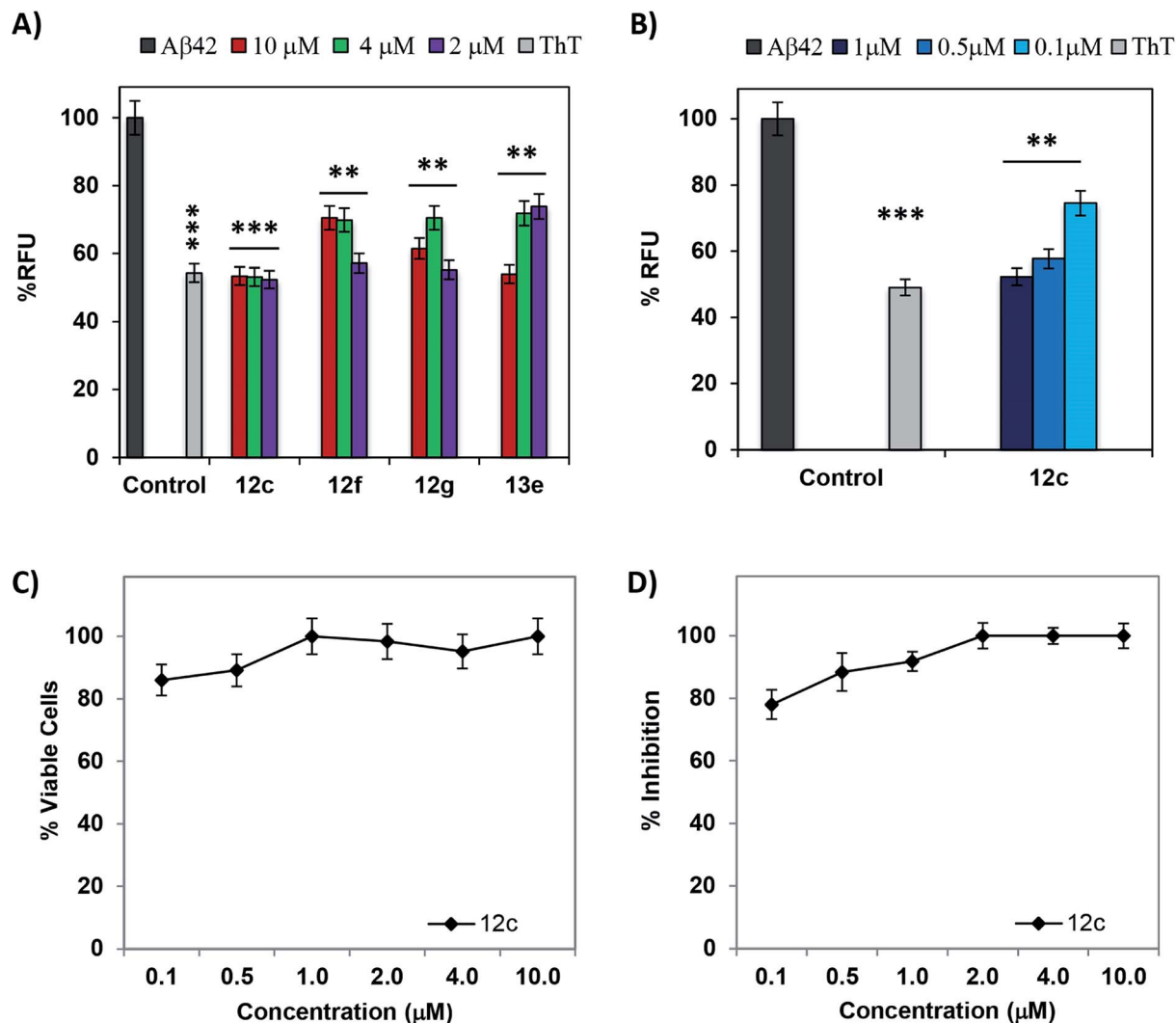


**Fig. 1** Effect of most active test peptides on Aβ<sub>42</sub> aggregation: bar plots depicting the decrease in % RFU of ThT dye when Aβ<sub>42</sub> (2 μM) was co-incubated with test peptides at higher doses (A), and lower doses (B). Complete fluorescence was represented by the Aβ<sub>42</sub> peptide incubated along with the dye (black) and dye control (grey) represents the dye incubated alone. Subsequent bars represent Aβ peptide co-incubated with the varying concentrations of inhibitor peptides for 24 h. Significance values indicated with respect to the Aβ peptides, \*,  $p < 0.05$ ; \*\*,  $p < 0.01$ ; \*\*\*,  $p < 0.001$ . (C) Dose dependent modulation of Aβ<sub>42</sub> aggregation-induced-neurotoxicity in PC-12 cells exhibited by the test peptide 12c (black). (D) Concentration dependent % inhibition on Aβ<sub>42</sub> aggregation mediated ThT fluorescence exhibited by the test peptide 12c (black). % inhibition of ThT fluorescence was calculated by using the formula:  $100 \times [100 - (\text{A}\beta_{42} + \text{test peptide RFU}_{485} - \text{control RFU}_{485}) / \text{A}\beta_{42} \text{ RFU}_{485} - \text{control RFU}_{485}]$ . Readings ( $\lambda_{\text{ex}}$  440 nm,  $\lambda_{\text{em}}$  485 nm) was recorded for triplicate samples from three individual experiments and the readings were averaged (<5% variation). Error bars represent mean  $\pm$  SD ( $n = 3$ ). Data were analyzed by one-way anova test.

Aβ<sub>42</sub>. Test peptide was added to each of the wells at the respective dose concentrations and readings were recorded at in a time dependent manner until 120 h of incubation. Time dependent % deformation of preformed fibrils in the presence of equimolar test peptide has been depicted in Fig. 4A. It could be observed that peptide 12c has the potential of deforming pre-aggregated Aβ<sub>42</sub> fibrils (>35%) until 48 h of incubation. Also, peptide 12c significantly reduced the fluorescence of Aβ<sub>42</sub> showing 57.5, 34.9 and 33.7% inhibition at 2, 1 and 0.5 μM, respectively after 24 h treatment. % inhibition and % RFU for time intervals of 24 h and 48 h has been provided in the ESI, Table S5.†

A time dependent ThT fluorescence assay was performed on the most active test peptide 12c at the similar concentrations of

2, 1 and 0.5 μM with Aβ<sub>42</sub> (2 μM) for a period of 7 days. Readings were recorded at regular time intervals of 24 h each. Fig. 4B shows the decrease in the RFU values when Aβ<sub>42</sub> was incubated in presence of peptide 12c. Aβ<sub>42</sub> on incubation alone with the ThT dye showed an enhancement in the fluorescence of about 57% that could be attributed to the aggregation of the Aβ<sub>42</sub> peptide. The fluorescence shown by the blank wells, wherein the dye incubated alone was considered as the control. Compared to the Aβ<sub>42</sub> sample, very low values of fluorescence were observed in the presence of peptide 12c. % inhibition of Aβ<sub>42</sub> aggregation exhibited by the test peptide has been summarized in ESI, Table S6.† It can be summed that peptide 12c exhibits activity on preformed Aβ<sub>42</sub> fibrils as well as inhibits Aβ<sub>42</sub> aggregation until 120 h of treatment.



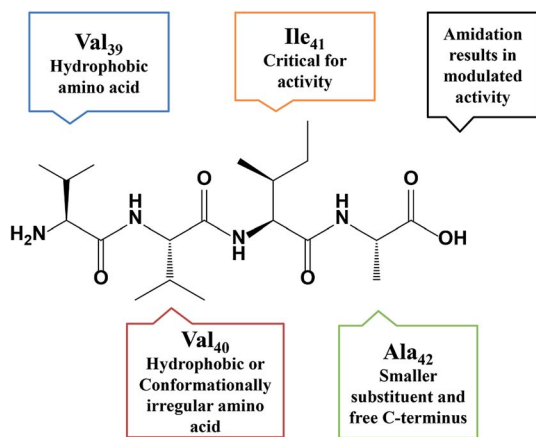


Fig. 2 Derived structure–activity-relationship of tetrapeptides.

ANS fluorescence assay was performed in complimentary to Thioflavin-T assay.<sup>27–29</sup> The effect of test peptide inhibiting the process of Aβ<sub>42</sub> aggregation as well as deformation of the pre-formed Aβ<sub>42</sub> fibrils was evaluated. The relative fluorescence for Aβ<sub>42</sub> fibrils was considered to be 100% and decrease in the % RFU when test peptides were co-incubated with Aβ<sub>42</sub> was computed. The fluorescence emitted by binding of ANS to the test peptide itself was subtracted as the test peptide is hydrophobic. The results for relative decrease in fluorescence obtained in both the sub-experiments have been summarized in Fig. 5A. Upon co-incubation of Aβ<sub>42</sub> and test peptide **12c** in ratios 1 : 1 and 1 : 0.5, a marked decrease in the fluorescence intensity was observed, in comparison to that of the lowest tested concentration of 0.5 μM. These results are in accordance to the results seen in ThT fluorescence assay.

It is hypothesized that the aggregated soluble oligomeric form of Aβ<sub>42</sub> interacts with the neuronal membranes by

hampering cellular processes and exhibiting neurotoxicity.<sup>7</sup> The design of the experiment was similar to the MTT test conditions, wherein giant unilamellar vesicles (GUVs) with composition mimicking the rat neuronal myelin were prepared (ESI,† Section 5.1) and interaction of Aβ was evaluated by ANS fluorescence measurements.<sup>29–32</sup> When Aβ<sub>42</sub> was just added to the prepared GUVs (*t* = 0 h), ANS showed a good emission spectrum from 450 to 550 nm. After 24 h incubation of Aβ with the vesicles, no emission band was seen, indicating the absence of hydrophobic binding domain, thus no fluorescence.

This could be attributed that the hydrophobic region entered the vesicles, providing no binding site for the dye. Emission intensities obtained for the vesicles alone was considered as blank and was subtracted from the readings obtained for both the time points. To evaluate the effects of incubation of test peptides and its inhibitory effect on Aβ<sub>42</sub> aggregation, Aβ<sub>42</sub> and test peptide **12c** along with the GUVs was incubated for 24 h at 37 °C and the relative change in the fluorescence was observed. Readings for the test peptide incubated alone with the vesicles at the similar concentration were subtracted the final readings so as to obtain a comparable result for Aβ. On co-incubation of Aβ<sub>42</sub> with **12c**, two distinct observations were seen, primarily a visible emission spectrum and secondly a blue shift with a slight increase in the emission intensity (Fig. 5B). The emission spectrum indicates that the hydrophobic region was available for binding to ANS, thus indicating that Aβ was available in its monomeric form itself. The increase in emission intensity and the blue shift does suggest certain interactions between **12c** and the full-length Aβ, which results into differential binding of ANS to the test peptide–Aβ complex (ESI, Fig. S2†).

Monitoring intrinsic Tyr fluorescence of Aβ<sub>42</sub> during fibril formation and interaction with most active test peptides was also studied. Tyr has significantly lower quantum yield than Trp

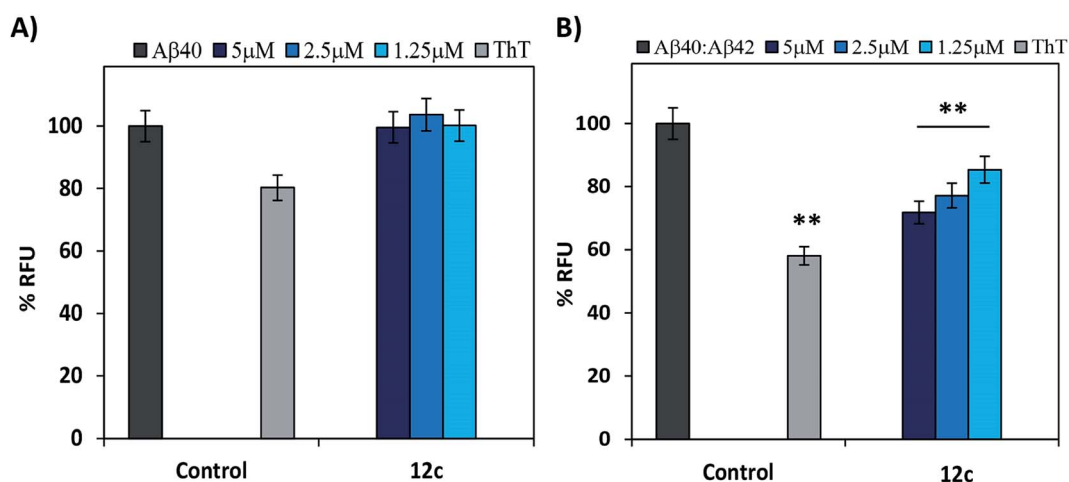


Fig. 3 Thioflavin-T fluorescence studies on Aβ species: % RFU exhibiting the effect of peptide **12c** on aggregation of (A) Aβ<sub>40</sub> (5 μM) and (B) Aβ<sub>40</sub> & Aβ<sub>42</sub> mixture (5 μM) mediated ThT fluorescence. Complete fluorescence was represented by Aβ<sub>40</sub> and the 10 : 1 mixture of Aβ peptides incubated along with the dye (black) and dye incubated alone (grey). Subsequent bars represent the respective concentrations of inhibitor peptide **12c** co-incubated with the corresponding Aβ peptides for 24 h. Readings ( $\lambda_{\text{ex}}$  440 nm,  $\lambda_{\text{em}}$  485 nm) was recorded for triplicate samples from three individual experiments and the readings were averaged (<5% variation). Error bars represent mean  $\pm$  SD (*n* = 3). Data were analyzed by one-way anova test. Significance values indicated with respect to the Aβ peptides, \*, *p* < 0.05; \*\*, *p* < 0.01; \*\*\*, *p* < 0.001.





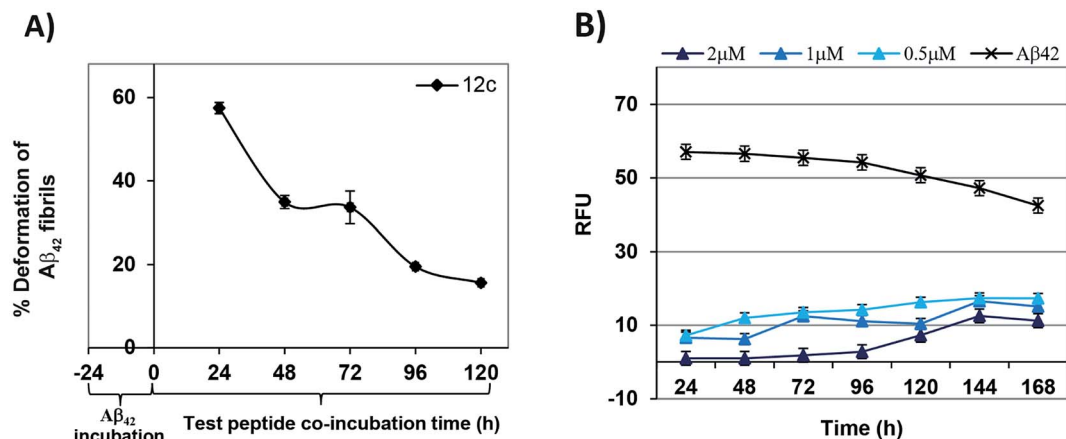


Fig. 4 Time dependent inhibition of Aβ<sub>42</sub>: (A) % deformation or disaggregation of preformed Aβ<sub>42</sub> fibrils in presence of equimolar concentration of test peptide 12c as evaluated via ThT fluorescence assay. (B) Time and concentration dependent RFU comparison depicting the effect of individual tetrapeptide 12c on Aβ<sub>42</sub> mediated-ThT fluorescence. % inhibition of ThT fluorescence was calculated by using the formula:  $100 \times [100 - (\text{A}\beta_{42} + \text{test peptide RFU}_{485} - \text{control RFU}_{485}) / \text{A}\beta_{42} \text{ RFU}_{485} - \text{control RFU}_{485}]$ . Readings ( $\lambda_{\text{ex}}$  440 nm,  $\lambda_{\text{em}}$  485 nm) was recorded for triplicate samples and the values were normalized to the ThT dye control and averaged (<5% variation). Data was interpreted from three individual experiments. Error bars represent mean  $\pm$  SD ( $n = 3$ ). Data were analyzed by one-way anova test.

and is usually only used as an intrinsic fluorescent probe in Trp-lacking proteins or peptides, since energy transfer to Trp residues usually quenches the Tyr fluorescence. Tyrosine shows a typical emission band at 305 nm, which is red shifted to 340 nm due to resonance of the phenol to phenolate ion. We hypothesized that in aggregated state of Aβ<sub>42</sub>, stacking of phenolate ions of the tyrosine residues will produce slightly enhanced fluorescence in comparison to that of the monomeric

or non-aggregated state. It could be clearly seen, in the overlay of fluorescence spectrum for Aβ<sub>42</sub> incubated alone for 0 h (green) and 24 h (black), as well as in presence of 12c (blue, Fig. 5C) that the monomeric state of Aβ<sub>42</sub> was retained in presence of the test peptides. A comparative bar plot analysis (ESI, Fig. S3†) of the fluorescence response at 340 nm has been indicated to compare the change in observed fluorescence intensities.

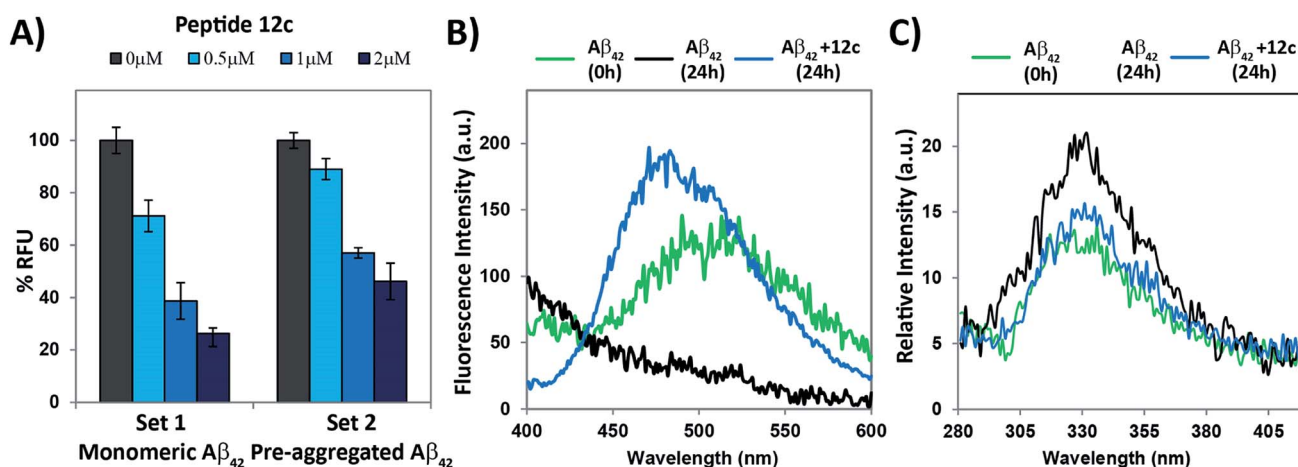


Fig. 5 Additional fluorescence studies: (A) effect of varying concentration of tetrapeptide 12c on inhibition of Aβ<sub>42</sub> fibril formation (Set 1) and on pre-aggregated fibrils of Aβ (Set 2). Complete fluorescence was represented by the Aβ<sub>42</sub> (2 μM) incubated alone, monomeric (Set 1) and pre-aggregated  $t = 24$  h (Set 2) and in the presence of respective concentrations of the test peptide 12c after 24 h. ANS dye incubated alone was considered as control and % RFU units for individual samples were computed by normalizing to the ANS dye control ( $\lambda_{\text{ex}}$  480 nm,  $\lambda_{\text{em}}$  535 nm). Subsequent bars represent the % RFU of the respective concentrations of the inhibitor peptide 12c co-incubated with the differential states of Aβ<sub>42</sub> peptide (2 μM) for 24 h. (B) Fluorescence spectrum showing effect of test peptide on Aβ<sub>42</sub> aggregation and its interaction with GUVs. Fluorescence of Aβ<sub>42</sub> alone at 0 h (green), 24 h (black); along with test peptides 12c (blue) after 24 h in the presence of GUVs ( $\lambda_{\text{ex}}$  480 nm,  $\lambda_{\text{em}}$  400–600 nm). ANS dye incubated alone was considered as control and relative FL. Intensities for individual samples were computed by normalizing to the ANS dye control. (C) Intrinsic tyrosine fluorescence of Aβ<sub>42</sub> during fibrillation and inhibition by test peptide 12c ( $\lambda_{\text{ex}}$  260 nm,  $\lambda_{\text{em}}$  280–410 nm). Fluorescence of 5 μM Aβ<sub>42</sub> ( $t = 0$  h, green), 5 μM Aβ<sub>42</sub> incubated alone ( $t = 24$  h, black), Aβ<sub>42</sub> co-incubated along with 5 μM of the test peptides, 12c ( $t = 24$  h, blue). Readings was recorded for triplicate samples from three individual experiments and were averaged (<5% variation). Error bars represent mean  $\pm$  SD ( $n = 3$ ). Data were analyzed by one-way anova test.



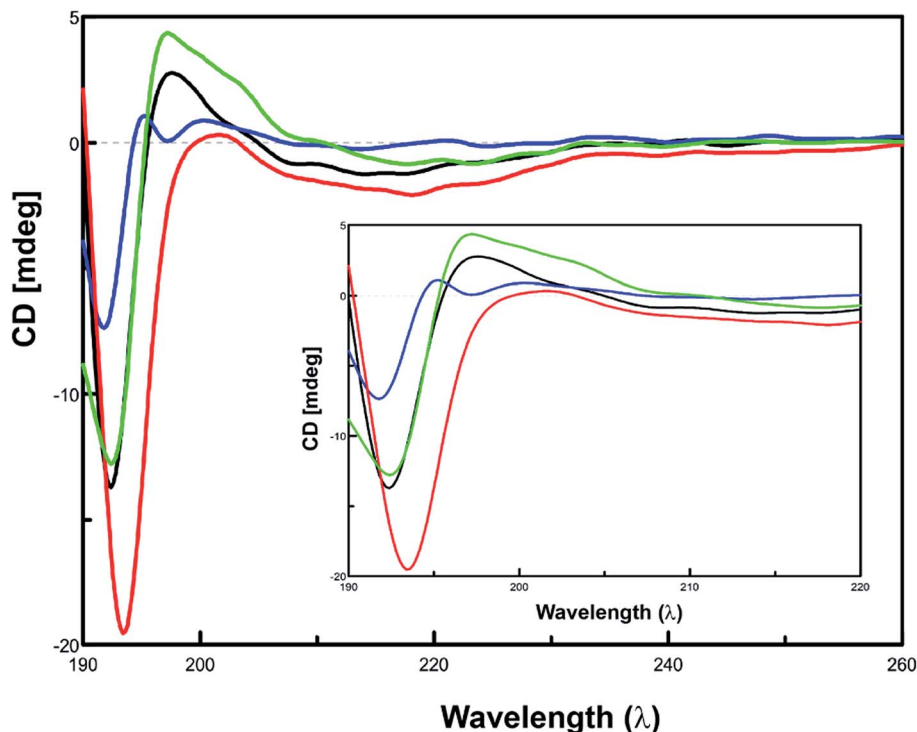


Fig. 6 Secondary structure analysis using CD: CD spectrum showing the conformational changes on  $A\beta_{42}$  aggregation in the presence of active peptide **12c** and inactive peptide **13a**.  $A\beta_{42}$  (10  $\mu$ M) at 0 h (black) and 24 h (blue), co-incubated individually with equimolar ratios inhibitor peptide **12c** (green) and inactive peptide **13a** (red) for 24 h.

Since amyloid- $\beta$  aggregation is preceded by the conformational transition towards increasing  $\beta$ -sheet structure, monitoring the content of  $\beta$ -sheet formation would therefore depict the effect of inhibitors on the aggregation of  $A\beta_{42}$ .<sup>32,33</sup> The effect of inhibitor peptides on the conformation of  $A\beta_{42}$  was assessed *via* CD spectroscopy.<sup>34–36</sup> Spectra of equimolar concentrations of the individual test peptides were subtracted from the corresponding spectra of inhibitor peptides co-incubated  $A\beta_{42}$ . Predicted values of conformation are summarized in ESI, Table S7.† When incubated alone,  $A\beta_{42}$  exhibited a conformational transition from random coiling and turn to majorly  $\beta$ -sheet form. Initially,  $A\beta_{42}$  peptide majorly comprised of 49.4%  $\beta$ -sheet conformation. At the end of 24 h incubation period,  $\beta$ -sheet content increased to 66.4%, with the  $\alpha$ -helix content increasing from 6.3% to 17.0%. In the presence of inhibitor peptide **12c**,  $\beta$ -sheet form completely vanished and turns and random coiling

was seen to be present in 46.6 and 41.0% respectively. This clearly indicates that **12c** inhibits  $\beta$ -sheet formation propensity of  $A\beta_{42}$ . The spectral curve obtained for  $A\beta_{42}$  ( $t = 24$  h) shows the presence of a positive maxima at 195 nm (black), clearly indicating the conformation of the peptide in the  $\beta$ -sheet form, is absent in the former that is,  $A\beta_{42}$  ( $t = 0$  h), which clearly exhibits a positive maxima at around 205 nm, indicating larger proportion of turn type conformation to be present. No definitive negative minima on the curve were visible at 217 nm, but the shallow curves in the expanded region were indicative of the presence of smaller proportions of  $\alpha$ -helix conformations. In the presence of **12c** reduction in  $\beta$ -sheet content can also be visualized by the complete absence of the positive maxima at 195 nm, wherein the spectrum follows the similar pattern to that of the  $A\beta_{42}$  ( $t = 0$  h). The prevention of conformational transition to  $\beta$ -sheet suggests the ability of **12c** to inhibit the

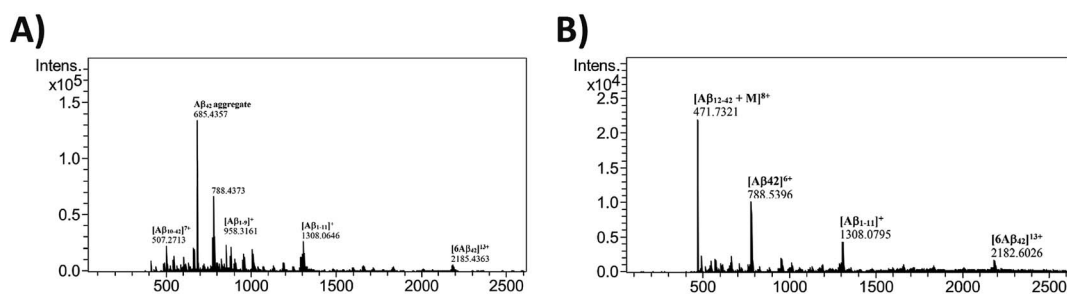


Fig. 7 HRMS Analysis: ESI-MS for  $A\beta_{42}$  (10  $\mu$ M) incubated alone (A), in presence of equimolar ratios of test peptide **12c** (B) for 24 h.



HR-TEM

STEM

HR-TEM

STEM

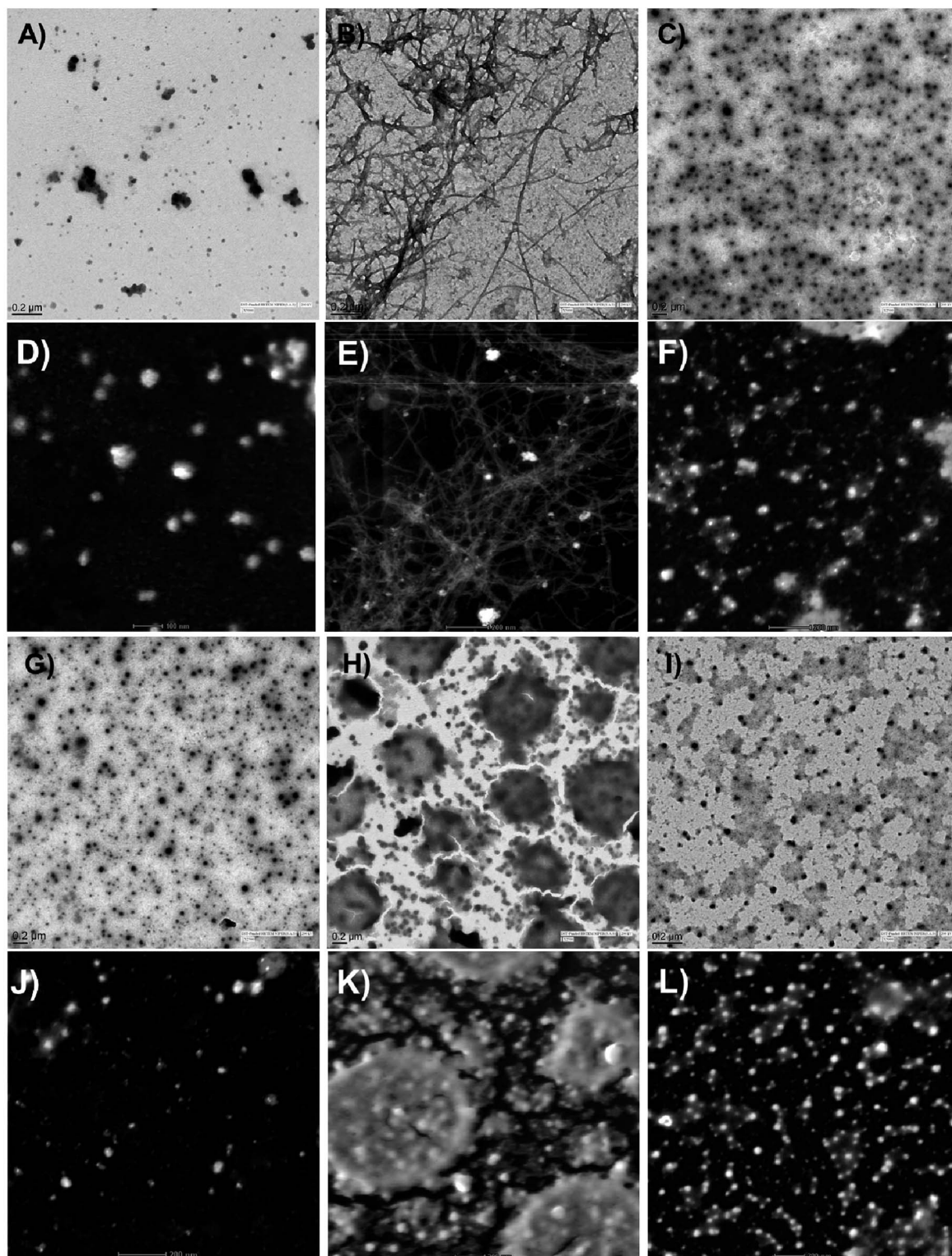


**Fig. 8** Electron microscopy studies: HR-TEM and STEM images depicting the effects of active peptide **12c** and inactive peptide **13a** on the aggregation of  $A\beta_{42}$ .  $A\beta_{42}$  ( $10\ \mu\text{M}$ ) was incubated alone  $t = 0\ \text{h}$  (A and D),  $t = 24\ \text{h}$  (B and E); with equimolar concentrations of inhibitor peptide **12c** (C and F); inactive peptide **13a** (H and K) as well as peptide **12c** (G and J) and inactive peptide **13a** (I and L) incubated alone, respectively. (Additional images have been provided in the ESI,<sup>†</sup> Section 11.3).

fibrillation process. The positive curve shifts more towards 200–205 nm, indicating a larger proportion of the peptide to be present in the turn form. These observations coincide to the

predicted values by the Yang protocol. The effect of the presence of equimolar concentrations of inactive peptide **13a** on the conformational changes on  $A\beta_{42}$  was evaluated. A positive





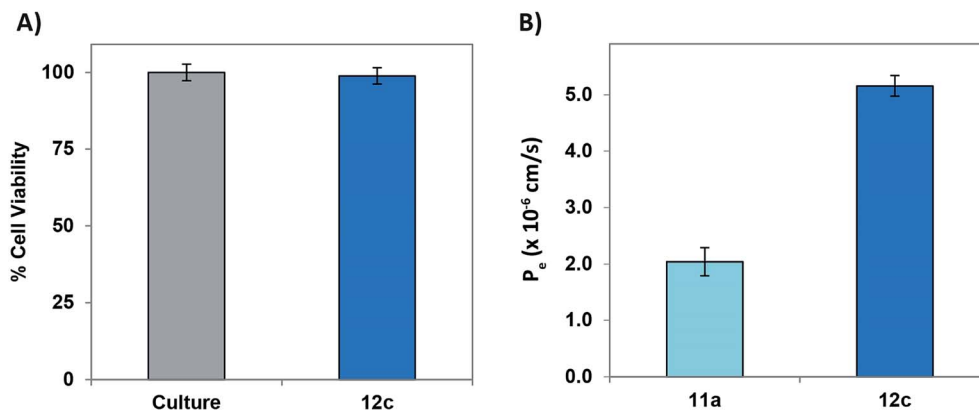


Fig. 9 Cytotoxicity and bioavailability study: (A) analysis of the cytotoxic effects of the peptide **12c** (20 mM) on the viability of PC-12 cells evaluated using MTT cell viability assay. The percentage of untreated cells was considered 100% (positive control) and presence of the test peptides in respective dose concentration for 6 h. (B) BBB-permeability of peptide **12c** in comparison to **11a**, as determined by the PAMPA-BBB assay.  $P_e$  was calculated by using the formula  $V_d V_a / [(V_d + V_a) S t] \ln(1 - A_a/A_e)$ , where  $V_d$  and  $V_a$  are the mean volumes of the donor and acceptor solutions,  $S$  is the surface area of the artificial membrane,  $t$  is the incubation time, and  $A_a$  and  $A_e$  are the UV absorbance of the acceptor well and the theoretical equilibrium absorbance, respectively. Data was recorded for triplicate samples in three individual experiments and the readings were averaged (<5% variation).

maxima at 195 nm is a clear indicative of higher proportions of  $\beta$ -sheet type of secondary structural conformation to be present. This indicates the inactiveness of the peptide **13a** and its inability to prevent aggregation of  $A\beta_{42}$ . Self-aggregation potential of peptide **13a** deters its potential to inhibit  $A\beta_{42}$  aggregation.

A compiled CD spectrum recorded depicting a relative comparison of peptides **12f** and **13a**, incubated for 24 h at 37 °C in the presence and absence of equimolar concentrations of  $A\beta_{42}$  has been presented in Fig. 6. Spectra of test peptides incubated alone were subtracted to obtain the final spectra for comparing the conformational state of  $A\beta_{42}$ . A comparison of the individual CD spectrums of the test peptides incubated alone to that incubated in the presence of equimolar ratio of  $A\beta_{42}$  has been summarized (ESI, Fig. S4†).

To understand the process of inhibition of  $A\beta_{42}$  in presence of **12c**, mass fragmentation techniques were employed.<sup>37</sup> The MS spectrum of full-length  $A\beta_{42}$  (10  $\mu$ M) in the presence and absence of an equimolar amount of **12c** was recorded. Fig. 7, shows the ESI spectrum for  $A\beta_{42}$  incubated alone (A), along with **12c** (B).

The spectrum for  $A\beta_{42}$  incubated alone shows a major peak at  $m/z$  685.4357, which may be attributed to aggregated  $A\beta_{42}$  depicting higher mass-to-charge ratio. Further peaks at  $m/z$  of 788.4373 [ $(A\beta_{42})_6^{6+}$ ], 507.2713 [ $(A\beta_{1-9})_1^{1+}$ ], 958.3161 [ $(A\beta_{10-42})_7^{7+}$ ] and 1308.0646 [ $(A\beta_{1-11})_1^{1+}$ ] represent the  $A\beta_{42}$  monomer and its specific fragments, respectively. Hexameric form of  $A\beta_{42}$  with  $m/z$  2185.4363 [ $(6A\beta_{42})_1^{13+}$ ] is also observed in the spectrum.<sup>38</sup> On comparing the spectrum obtained for  $A\beta_{42}$  incubated along with **12c**, and that of  $A\beta_{42}$  incubated alone, additional signal peaks were seen. This suggested the occurrence of adduct between  $A\beta_{42}$  and **12c**, as these peaks were not analogous to the molecular weight of native  $A\beta_{42}$  or test peptides themselves. Analyzing the interactions of **12c** with that of  $A\beta_{42}$ , the mass spectrum shows a peak at  $m/z$  471.7321 [ $(A\beta_{12-42} + 12c)_8^{8+}$ ],

depicting 1 : 1 covalent interaction with  $A\beta_{12-42}$  fragment of  $A\beta_{42}$ . The spectrum also shows signal peaks corresponding to that of  $A\beta_{42}$ , seen in the previous spectrum. It was clear from the above spectrum that the test peptide interacts with the monomeric unit of the  $A\beta_{42}$ , thereby preventing its aggregation.

Visual investigation of the effects of the peptide **12c**, on the morphology and abundance of  $A\beta_{42}$  fibrils was performed by high resolution transmission electron microscopy (HR-TEM).<sup>39</sup> Shapes and morphology of the fibrils were also examined using scanning transmission electron microscope (STEM).<sup>40</sup> Inactive peptide **13a** was selected as a negative control. The control sample of  $A\beta_{42}$  incubated alone at  $t = 0$  h, where uniform distribution of smaller particles of  $A\beta$  was seen (Fig. 8A, HR-TEM and Fig. 8D, STEM).

After an incubation span of 24 h, appearance of amyloid fibrils and an extensive network of long, straw-shaped fibrils were observed (Fig. 8B and E). In the presence of peptide **12c** (Fig. 8C and F), only smaller particulate aggregates were seen, indicating complete inhibition of the amyloid fibrils. On co-incubation of  $A\beta_{42}$  with the inactive peptide **13a**, large aggregated structures (Fig. 8H and K) were observed. In order to visualize the aggregation of the peptide themselves, equimolar concentrations of peptides **12c** and **13a** were incubated alone under similar conditions and visualized. Very small granular structures were seen for the **12c** (Fig. 8G and J) whereas slightly larger and patchy aggregates were seen for inactive peptide **13a** (Fig. 8I and L).

In order to evaluate and understand the biosafety and pharmacokinetic profile of the test peptides, cell-cytotoxicity studies employing PC-12 cells was performed. Test peptide were tested up to a highest tested concentration of 20  $\mu$ M and none of the peptides exhibited undesirable cytotoxicity. Fig. 9A depicts a graphical representation of the % viable cells in presence of 20  $\mu$ M concentration of peptide **12c**.



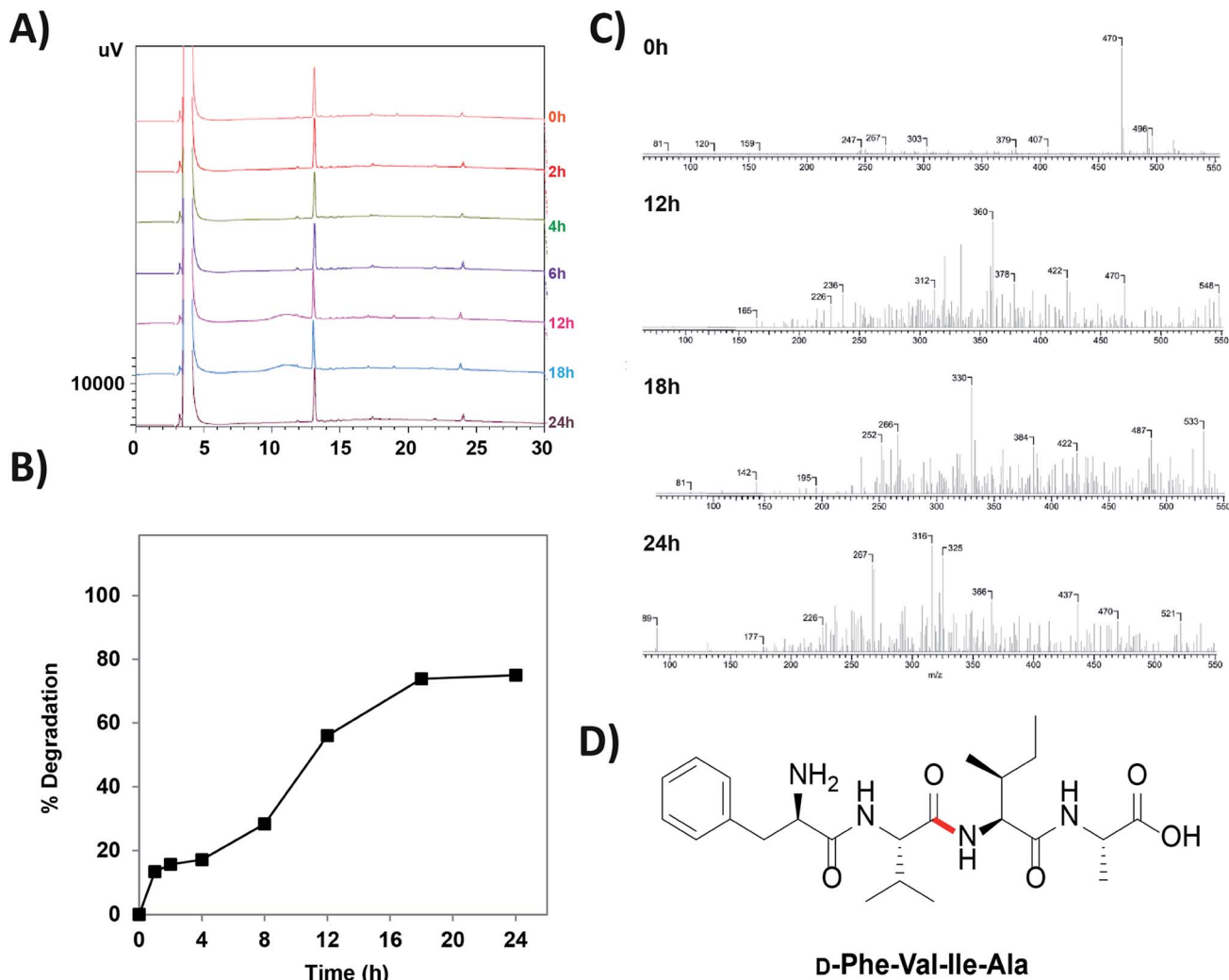


Fig. 10 Proteolytic stability study: (A) superimposed HPLC chromatograms of most active peptide 12c at time intervals of 0, 2, 4, 8, 12, 18 and 24 h after trypsin treatment; (B) graphical representation showing % degradation for peptide 12c on serum treatment. (C) Mass spectra for peptide 12c at 0, 12, 18 and 24 h of serum treatment. Analyzed by ACD-Mass Fragmenter tool. (D) Predicted susceptible cleavage sites for peptide 12c. Most susceptible peptide bond has been indicated in bold red.

A major challenge for peptide-based therapeutics is the BBB permeability and proteolytic stability against various enzymes within the body.<sup>41</sup> *In vitro* BBB penetration of the most active peptide 12c as well as the lead peptide 11a using parallel artificial membrane permeation assay (PAMPA-BBB) was performed following the previously reported protocols.<sup>42–45</sup> The UV/Vis absorptions of both the peptides was recorded after permeating through an artificial porcine polar brain lipid (PBL) membrane and the effective permeabilities ( $P_e$ ) were calculated. As described in Fig. 9B, the  $P_e$  values of the most active peptide 12c was significantly higher than that of 11a, demonstrating enhanced permeability of the modified peptide.

Trypsin is the one of the most notorious endopeptidases and cleaves the amide bond next to a charged cationic residue.<sup>46</sup> Hence, in order to evaluate whether the synthesized peptides have incorporated the proteolytic stability properties, trypsin and serum stability studies on the peptide 12c was performed. The peptide was incubated with 100-fold excess of trypsin and

was subjected to analysis by RP-HPLC. Chromatograms depicted that the peptides exhibited intact integrity, having their retention time unaltered even after 24 h of trypsin treatment. It was observed that, there were no peaks seen before and after the main peak of the peptide indicating no fragment and/or other intermediate formation. Superimposed HPLC chromatograms of time point's intervals have been depicted in Fig. 10A.

Serum stability assay following similar protocol was performed. The chromatograms depicted that the peptides exhibited intact integrity, having their retention time unaltered up to 12 h of serum treatment. The peaks obtained for the peptides at 18 h and 24 h of serum treatment, were comparatively smaller to that of the previous peaks indicating slight degradation of the peptide. Superimposed HPLC chromatogram for peptide 12c has been provided in ESI, Fig. S6.†

To calculate the rate of degradation of the peptide on serum treatment, analysis and comparison the area under the curve of the peak of the respective peptide at their specific time



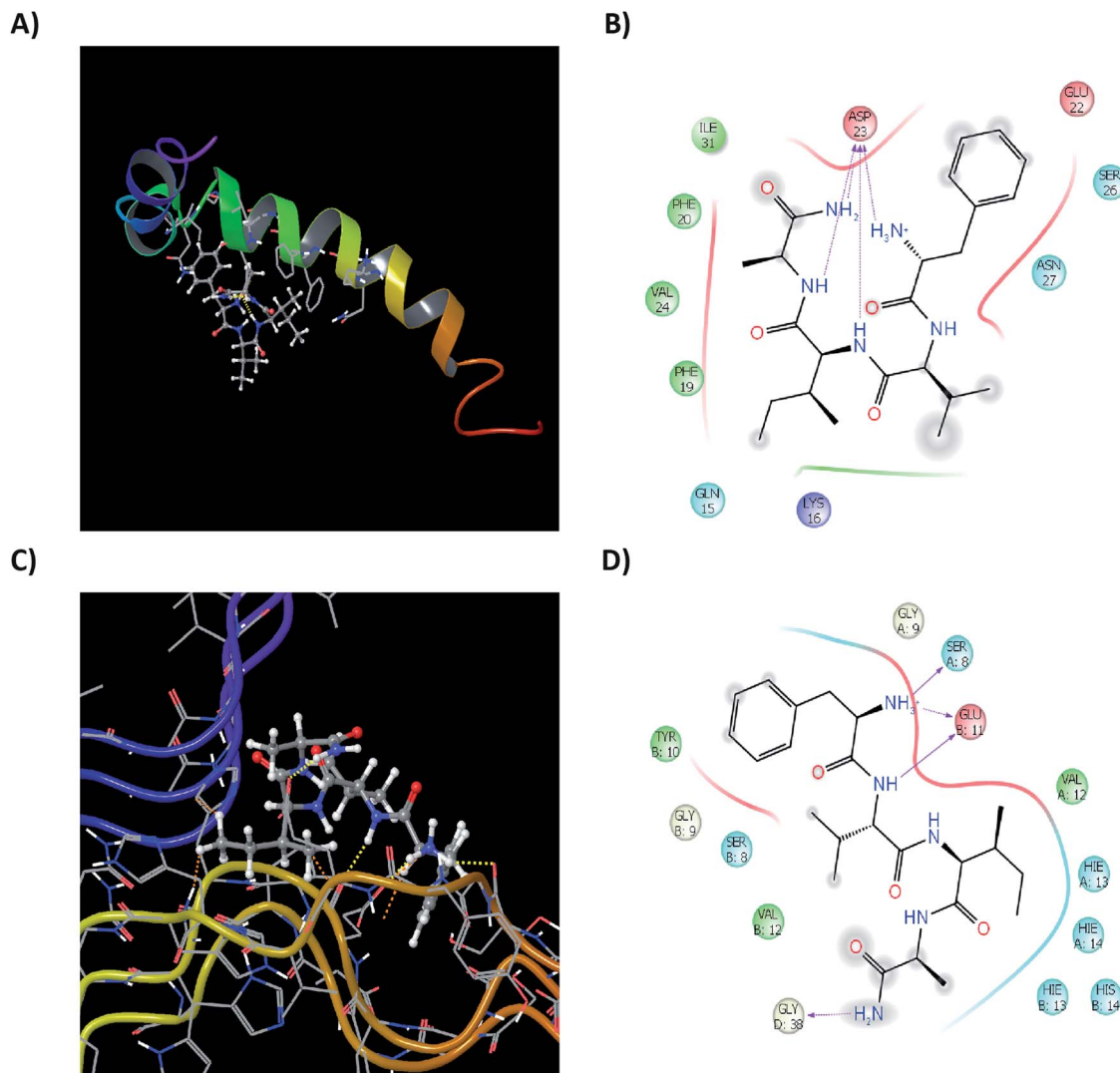


Fig. 11 *In silico* study: ligand interaction diagram showing interactions of the ligand with the residues of monomeric unit 1IYT-10 (A and B) and with the proto-fibrillar unit 2NAO-06 (C and D). 3D representation (Left) showed along with 2D representation (Right).

intervals.<sup>47,48</sup> A comparative analysis depicted that around 20% of the peptide is present after 24 h of serum treatment. Fig. 10B indicates the % degradation of the peptide in serum over a period of 24 h. The initial calculation of % peptide present in the sample aliquot is indicated in the ESI, Fig. S7†. The extrapolated data helped us to determine the degradation rate of the peptide in serum (ESI, Table S8†).<sup>48–50</sup> It can be concluded that approximately 50% of the peptide is stable until 12 h of serum treatment, following which it shows a decline in stability decreasing to about 22% until 24 h.

In order to study the mode of degradation of the peptide and the susceptibility of the peptide towards peptide degradation, mass spectroscopy was employed. The samples analyzed for peptide content on RP-HPLC were further subjected to LCQ analysis.<sup>51,52</sup> At 0 h, the molecular ion peak ( $m/z$  470) of the peptide corresponded to the molecular mass of the peptide itself. Sequential fragmentation pattern was minimal and a clear mass spectrum was seen. After 12 h, multiple

fragmentation peaks were seen indicating that the peptide has undergone cleavage at multiple sites. ACD-Mass Fragmenter tool was used to analyze the specific fragmentation pattern. Fig. 10C summarizes the mass spectrums and shows the specific fragmentation pattern. Based on the fragmentation pattern for the tetrapeptide sequence, the most susceptible bonds that could easily undergo cleavage were identified. ACD Mass Fragmenter tool was used to understand the peptide fragmentation pattern. Fig. 10D depicts the structure of the peptide 12c indicating the most susceptible peptide bond. This understanding provides impetus in site specific modification in improving the stability of the peptides.

Computationally understanding the binding mechanism and intra-residual interactions of the test peptides with the single monomeric as well as the proto-fibrillar unit of A $\beta$ <sub>42</sub> would prove to be useful. Various structures for the both the forms of A $\beta$ <sub>42</sub> are reported in the literature. A monomeric sequence bearing complete sequence of all 42 amino acids



residues was used (PDB Id: 1IYT; ESI, Fig. S8†). The structure comprises of  $\alpha$ -helices and random coiling, similar to the data previously reported.<sup>53</sup> A proto-fibrillar unit comprising of 6 full length spatially arranged in a 'S' shaped manner recently reported by Colvin and co-workers<sup>54</sup> (PDB Id: 2NAO, ESI, Fig. S10†) was used for understanding the interaction of the test peptides on the proto-fibrillar unit of A $\beta$ . Reactive site analysis of the pre-optimized framework of the monomeric A $\beta$ <sub>42</sub> showed that the hinge region is the most prone to aggregation due to the presence of reactive residues in that particular segment (Maestro, Bioluminate suite; ESI Fig. S9†). To understand the interaction of the test peptide with the full-length A $\beta$ <sub>42</sub>, a grid incorporating the whole sequence was generated. Docking studies were performed with the peptides mentioned in this work along with a few molecules reported in literature<sup>10–12,55,56</sup> for comparative analysis of the binding modes and interactions.<sup>57–59</sup> Docking, glide and residual interaction energy scores for the molecules selected from literature and test peptides from the current study are summarized in ESI (Tables S9 and S10†). Although the analysis of the scores reveal that similar docking and glide scores were seen in both the cases. The energy of interaction of the test peptides with the monomeric unit proved to be a comparable factor to that of the literature reported ligands (ESI Table S11†).

Test peptides have shown to interact with Glu<sub>11</sub>, His<sub>13</sub>, His<sub>14</sub>, Gln<sub>15</sub>, Phe<sub>19</sub>, Phe<sub>20</sub> and more specifically with Asp<sub>23</sub>. These residues are involved to aid the aggregation of monomeric A $\beta$ <sub>42</sub> into the fibrillar species, as also seen in reactive residue analysis (ESI, Fig. S11†). Binding of the test peptides to these residues, block the free interaction of these residues to others, inhibiting their aggregation propensity. Ligand interactions of the most active test peptide **12c** with the monomeric unit, their respective ligand interaction diagrams (2D and 3D) have been summarized in Fig. 11A and B. The interaction energies are in accordance to those exhibited by the standard ligands indicating similar kind of interactions and thus reinforcing the results of studies carried out in this work. A structural framework 2NAO-06 of proto-fibrillar A $\beta$ <sub>42</sub> was rationalized to be the most optimal structure and was prepared for docking studies (ESI, Fig. S10†). Since it is a proto-fibrillar unit, the most reactive sites for the binding were identified. SiteMap Analysis feature identified 5 ligand-binding sites (ESI, Fig. S12†). The predicted sites did coincide with the predicted reactive residues, thus indicating certain interactions between those residues and the ligand to be feasible, which would inhibit the process of aggregation. To carry out docking studies, receptor grids at the predicted sites on the proto-fibrillar unit was generated. Since there has been no docking studies performed using 2NAO as the protein, validation of the use of 2NAO and the predicted sites, by docking standard ligands was performed (ESI, Tables S12 and S13†). Analysis of the docking studies revealed SiteMap-2 to be the most plausible site for action of an inhibitor. The molecule can interact with the residues that aid in aggregation. This would block the further attachment of another monomeric unit to the site-recognition units on the proto-fibrillar structure. Subsequent interaction with the neighboring residues of both

the chains destabilizes the preformed bonds, which hold the adjacent units together.

Docking studies of the peptides presented in this work was carried out and docking scores and the residue interaction energies obtained for the set of synthesized tetrapeptides for SiteMap-2 has been summarized in ESI, Table S14.† On careful analysis it can be seen that interaction with Met<sub>35</sub>, Val<sub>36</sub>, Gly<sub>37</sub> of chain D, as well as Glu<sub>11</sub>, His<sub>13</sub>, His<sub>14</sub> and Gln<sub>15</sub> of the neighboring chain A, show that the test peptide does interact with both the neighboring chains and especially with those amino acids that are solely responsible for maintaining the dimeric structure of the proto-fibrillar unit. To have a clear understanding of the interactions, ligand interaction diagrams for the test peptide **12c**, depicting its interaction with the specific residues of the proto-fibrillar unit have been summarized in Fig. 11C and D.

## Conclusion

The peptides described herein show potent inhibition against amyloid aggregation and A $\beta$ <sub>42</sub> mediated neurotoxicity. Thioflavin-T, ANS and tyrosine fluorescence assays support the results and depict the inhibitory potential of the reported peptides. Inferences from CD studies show that peptide **12c** has  $\beta$ -sheet breaking ability, which was also visually inspected by the absence of A $\beta$ <sub>42</sub> fibrils in the electron microscopy experiments. Amidated C-terminus protection is a well utilized concept and has enhanced stability of peptide-based therapeutics. Improved BBB permeation along with proteolytic and serum stability parameters provide the designed compounds an attractive biological profile. Peptide **12c** bind to the parent peptide in its monomeric as well as proto-fibrillar form, which aids in inhibiting the process of aggregation as well as destabilization of the preformed fibrils as perceived by *in silico* studies. Excellent potency, enhanced permeability, negligible cytotoxicity along with optimal biological profile, dictate that peptide **12c** is an interesting lead as anti-Alzheimer's disease agent. This study provides further impetus to rational design and development of peptide-based therapeutics for AD.

## Abbreviations

A $\beta$ <sub>40</sub>	Amyloid- $\beta$ <sub>1–40</sub>
A $\beta$ <sub>42</sub>	Amyloid- $\beta$ <sub>1–42</sub>
AD	Alzheimer's disease
Aib	$\alpha$ -Aminoisobutyric acid
APCI	Atmospheric pressure chemical ionization
CD	Circular dichroism
HRMS	High resolution mass spectrometry
HR-TEM	High resolution-transmission electron microscopy
MTT	[3-(4,5-Dimethylthiazol-2-yl)-2'-5'-diphenyltetrazolium] bromide
MW	Microwave
Nm	Nanometer
OD	Optical density





PBS	Phosphate buffered saline
PC-12	Pheochromocytoma-12 cells
RFU	Relative fluorescence unit
RP-HPLC	Reverse-phase high performance liquid chromatography
rt	Room temperature
SAR	Structure–activity relationship
SD	Standard deviation
SPPS	Solid phase peptide synthesis
STEM	Scanning transmission electron microscopy
TBTU	O-(Benzotriazol-1-yl)-N,N,N',N'-tetramethyluronium tetrafluoroborate
TFA	Trifluoroacetic acid
TFE	Trifluoroethanol
ThT	Thioflavin-T
TIPS	Triisopropylsilane
$t_R$	Retention time (in chromatography)
UV	Ultraviolet

## Conflicts of interest

The authors declare no competing financial interest.

## Acknowledgements

AK would like to thank Mihir Khambete for his valuable suggestions. Central Instrumentation Laboratory and DST funded HR-TEM facility at NIPER is duly acknowledged.

## References

- 1 J. Gaugler, B. James, T. Johnson, A. Marin and J. Weuve, 2019 Alzheimer's disease facts and figures, *Alzheimer's Dementia*, 2019, **15**, 321–387.
- 2 J. Hardy and G. Higgins, Alzheimer's disease: the amyloid cascade hypothesis, *Science*, 1992, **256**, 184–186.
- 3 Alzheimer's Association, *Alzheimer's Disease Facts and Figures*, 2019, Please see: <http://www.alz.org/facts/>, accessed on 20.05.2020.
- 4 J. Cummings, G. Tong and C. Ballard, Treatment combinations for Alzheimer's disease: Current and future pharmacotherapy options, *J. Alzheimer's Dis.*, 2019, **67**, 779–794.
- 5 D. Wong, P. Rosenberg, P. Zhou, A. Kumar, V. Raymont, H. Ravert, R. F. Dannals, A. Nandi, J. Brašić, W. Ye and J. Hilton, In vivo imaging of amyloid deposition in Alzheimer disease using the radioligand 18F-AV-45 (flobetapir F-18), *J. Nucl. Med.*, 2010, **51**, 913–920.
- 6 R. Anand, K. Gill and A. Mahdi, Therapeutics of Alzheimer's disease: Past, present and future, *Neuropharmacol*, 2014, **76**, 27–50.
- 7 S. Lee, E. Nam, H. Lee, M. Savelieff and M. Lim, Towards an understanding of amyloid- $\beta$  oligomers: characterization, toxicity mechanisms, and inhibitors, *Chem. Soc. Rev.*, 2017, **75**, 333–366.
- 8 F. Aileen and D. Willbold, Peptides for therapy and diagnosis of Alzheimer's disease, *Curr. Pharm. Des.*, 2012, **18**, 755–767.
- 9 N. Sun, S. Funke and D. Willbold, A survey of peptides with effective therapeutic potential in Alzheimer's disease rodent models or in human clinical studies, *Mini-Rev. Med. Chem.*, 2012, **12**, 388–398.
- 10 S. Bansal, I. Maurya, N. Yadav, C. Thota, V. Kumar, K. Tikoo, S. Chauhan and R. Jain, C-Terminal fragment, A $\beta_{32-37}$ , analogues protect against A $\beta$  aggregation-induced toxicity, *ACS Chem. Neurosci.*, 2016, **7**, 615–623.
- 11 S. Bansal, I. Maurya, K. Shenmar, N. Yadav, C. Thota, V. Kumar, K. Tikoo, S. Chauhan and R. Jain, A $\beta_{1-42}$  C-terminus fragment derived peptides prevent the self-assembly of the parent peptide, *RSC Adv.*, 2017, **7**, 4167–4173.
- 12 S. Bansal, I. Maurya, K. Shenmar, N. Yadav, C. Thota, V. Kumar, K. Tikoo, S. Chauhan and R. Jain, C-Terminal fragment, A $\beta_{39-42}$ -based tetrapeptides mitigates amyloid- $\beta$  aggregation induced toxicity, *ACS Omega*, 2018, **3**, 10019–10032.
- 13 M. Shearman, S. Hawtin and V. Tailor, The intracellular component of cellular 3-(4,5-dimethylthiazol-2-yl)-2,5-diphenyltetrazolium bromide (MTT) reduction is specifically inhibited by  $\beta$ -amyloid peptides, *J. Neurochem.*, 1995, **65**, 218–227.
- 14 M. Krebs, E. Bromley and A. Donald, The binding of thioflavin-T to amyloid fibrils: localization and implications, *J. Struct. Biol.*, 2005, **149**, 30–37.
- 15 T. Ban, D. Hamada, K. Hasegawa, H. Naiki and Y. Goto, Direct observation of amyloid fibril growth monitored by thioflavin T fluorescence, *J. Biol. Chem.*, 2003, **278**, 16462–16465.
- 16 C. Xue, T. Lin, D. Chang and Z. Guo, Thioflavin T as an amyloid dye: fibril quantification, optimal concentration and effect on aggregation, *R. Soc. Open Sci.*, 2017, **4**, 160696.
- 17 M. Gessel, C. Wu, H. Li, G. Bitan, J. Shea and M. Bowers, A $\beta_{(39-42)}$  modulates A $\beta$  oligomerization but not fibril formation, *Biochemistry*, 2011, **51**, 108–117.
- 18 S. Gandy, The role of cerebral amyloid- $\beta$  accumulation in common forms of Alzheimer disease, *J. Clin. Invest.*, 2005, **115**, 1121–1129.
- 19 M. Citron, T. Diehl, G. Gordon, A. Biere, P. Seubert and D. Selkoe, Evidence that the 42-and 40-amino acid forms of amyloid  $\beta$  protein are generated from the  $\beta$ -amyloid precursor protein by different protease activities, *Proc. Natl. Acad. Sci. U. S. A.*, 1996, **93**, 13170–13175.
- 20 D. Borchelt, G. Thinakaran, C. Eckman, M. Lee, F. Davenport, T. Ratovitsky, C. Prada, G. Kim, S. Seekins, D. Yager and H. Slunt, Familial Alzheimer's disease – linked presenilin 1 variants elevate A $\beta_{1-42/1-40}$  ratio *in vitro* and *in vivo*, *Neuron*, 1996, **17**, 1005–1013.
- 21 K. Fassbender, M. Simons, C. Bergmann, M. Stroick, D. Lütjohann, P. Keller, H. Runz, S. Kühl, T. Bertsch, K. Von Bergmann and M. Hennerici, Simvastatin strongly reduces levels of Alzheimer's disease  $\beta$ -amyloid peptides A $\beta_{42}$  and A $\beta_{40}$  *in vitro* and *in vivo*, *Proc. Natl. Acad. Sci. U. S. A.*, 2001, **98**, 5856–5861.



- 22 S. Tomski and R. Murphy, Kinetics of aggregation of synthetic  $\beta$ -amyloid peptide, *Arch. Biochem. Biophys.*, 1992, **294**, 630–638.
- 23 D. Gordon, K. Sciarretta and S. Meredith, Inhibition of  $\beta$ -amyloid<sub>(40)</sub> fibrillogenesis and disassembly of  $\beta$ -amyloid<sub>(40)</sub> fibrils by short  $\beta$ -amyloid congeners containing N-methyl amino acids at alternate residues, *Biochemistry*, 2001, **40**, 8237–8245.
- 24 B. Taylor, R. Sarver, G. Fici, R. Poorman, B. Lutzke, A. Molinari, T. Kawabe, K. Kappenman, A. Buhl and D. Epps, Spontaneous aggregation and cytotoxicity of the  $\beta$ -amyloid A $\beta$ <sub>1–40</sub>: a kinetic model, *J. Protein Chem.*, 2003, **22**, 31–40.
- 25 Q. Wang, X. Yu, K. Patal, R. Hu, S. Chuang, G. Zhang and J. Zheng, Tanshinones inhibit amyloid aggregation by amyloid- $\beta$  peptide, disaggregate amyloid fibrils, and protect cultured cells, *ACS Chem. Neurosci.*, 2013, **4**, 1004–1015.
- 26 L. Lee, H. Ha, Y. Chang and M. DeLisa, Discovery of amyloid-beta aggregation inhibitors using an engineered assay for intracellular protein folding and solubility, *Protein Sci.*, 2009, **18**, 277–286.
- 27 O. Gasyimov and B. Glasgow, ANS fluorescence: Potential to augment the identification of the external binding sites of proteins, *Biochim. Biophys. Acta, Proteins Proteomics*, 2007, **1774**, 403–411.
- 28 M. Lindgren, K. Sörgjerd and P. Hammarström, Detection and characterization of aggregates, prefibrillar amyloidogenic oligomers, and protofibrils using fluorescence spectroscopy, *Biophys. J.*, 2005, **88**, 4200–4212.
- 29 P. Alam, M. Siddiqi, S. Chaturvedi, M. Zaman and R. Khan, Vitamin B12 offers neuronal cell protection by inhibiting A $\beta$ <sub>42</sub> amyloid fibrillation, *Int. J. Biol. Macromol.*, 2017, **99**, 477–482.
- 30 A. Saha, G. Mondal, A. Biswas, I. Chakraborty, B. Jana and S. Ghosh, *In vitro* reconstitution of a cell-like environment using liposomes for amyloid beta peptide aggregation and its propagation, *Chem. Commun.*, 2013, **49**, 6119–6121.
- 31 Y. Verdier, M. Zarándi and B. Penke, Amyloid  $\beta$  peptide interactions with neuronal and glial cell plasma membrane: binding sites and implications for Alzheimer's disease, *J. Pept. Sci.*, 2004, **10**, 229–248.
- 32 L. Simmons, P. May, K. Tomaselli, R. Rydel, K. Fuson, E. Brigham, S. Wright, I. Lieberburg, G. Becker and D. Brems, Secondary structure of amyloid beta peptide correlates with neurotoxic activity in vitro, *Mol. Pharmacol.*, 1997, **45**, 373–379.
- 33 Y. Feng, X. Wang, S. Yang, Y. Wang, X. Zhang, X. Du, X. Sun, M. Zhao, L. Huang and R. Liu, Resveratrol inhibits beta-amyloid oligomeric cytotoxicity but does not prevent oligomer formation, *Neurotoxicology*, 2009, **30**, 986–995.
- 34 T. Harada and R. Kuroda, CD measurements of  $\beta$ -amyloid (1–40) and (1–42) in the condensed phase, *Biopolymers*, 2011, **95**, 127–134.
- 35 D. K. Weber, J. D. Gehman, F. Separovic and M. A. Sani, Copper modulation of amyloid beta 42 interactions with model membranes, *Aust. J. Chem.*, 2012, **65**, 472–479.
- 36 M. Pappolla, P. Bozner, C. Soto, H. Shao, N. K. Robakis, M. Zagorski, B. Frangione and J. Ghiso, Inhibition of Alzheimer  $\beta$ -fibrillogenesis by melatonin, *J. Biol. Chem.*, 1998, **273**, 7185–7188.
- 37 S. Chimon, M. Shaibat, C. Jones, D. Calero, B. Aizezi and Y. Ishii, Evidence of fibril-like  $\beta$ -sheet structures in a neurotoxic amyloid intermediate of Alzheimer's  $\beta$ -amyloid, *Nat. Struct. Mol. Biol.*, 2007, **14**, 1157–1164.
- 38 S. Bernstein, N. Dupuis, N. Lazo, T. Wytenbach, M. Condron, G. Bitan, D. Teplow, J. Shea, B. Ruotolo, C. Robinson and M. Bowers, Amyloid- $\beta$  protein oligomerization and the importance of tetramers and dodecamers in the etiology of Alzheimer's disease, *Nat. Chem.*, 2009, **1**, 326–331.
- 39 T. Shirahama and A. Cohen, High-resolution electron microscopic analysis of the amyloid fibril, *J. Cell Biol.*, 1967, **33**, 679–708.
- 40 D. Eisenberg and M. Sawaya, Structural Studies of Amyloid Proteins at the Molecular Level, *Annu. Rev. Biochem.*, 2017, **86**, 69–95.
- 41 D. Craik, D. Fairlie, S. Liras and D. Price, The future of peptide-based drugs, *Chem. Biol. Drug Des.*, 2013, **81**, 136–147.
- 42 W. Banks, Peptides and the blood–brain barrier, *Peptides*, 2015, **72**, 16–19.
- 43 M. Li, Y. Dong, X. Yu, Y. Li, Y. Zou, Y. Zheng, Z. He, Z. Liu, J. Quan, X. Bu and H. Wu, Synthesis and Evaluation of Diphenyl Conjugated Imidazole Derivatives as Potential Glutamyl Cyclase Inhibitors for Treatment of Alzheimer's Disease, *J. Med. Chem.*, 2017, **60**, 6664–6677.
- 44 P. Camps, X. Formosa, C. Galdeano, D. Munoz-Torrero, L. Ramirez, E. Gomez, N. Isambert, R. Lavilla, A. Badia, M. Clos, M. Bartolini, F. Mancini, V. Andrisano, M. Arce, M. Rodriguez-Franco, O. Huertas, T. Dafni and F. Luque, Pyrano[3,2-c]quinoline-6-chlorotacrine hybrids as a novel family of acetylcholinesterase- and beta-amyloid-directed anti-Alzheimer compounds, *J. Med. Chem.*, 2009, **52**, 5365–5379.
- 45 L. Di, E. Kerns, K. Fan, O. McConnell and G. Carter, High throughput artificial membrane permeability assay for blood–brain barrier, *Eur. J. Med. Chem.*, 2003, **38**, 223–232.
- 46 D. Hook, P. Bindschädler, Y. Mahajan, R. Šebesta, P. Kast and D. Seebach, The proteolytic stability of 'designed' $\beta$ -peptides containing  $\alpha$ -peptide-bond mimics and of mixed  $\alpha$ ,  $\beta$ -peptides: application to the construction of MHC-binding peptides, *Chem. Biodiversity*, 2005, **2**, 591–632.
- 47 V. Demidov, V. Potaman, M. Frank-Kamenetskii, M. Egholm, O. Buchard, S. Sönnichsen and P. Nielsen, Stability of peptide nucleic acids in human serum and cellular extracts, *Biochem. Pharmacol.*, 1994, **48**, 1310–1313.
- 48 C. Adessi, M. Frossard, C. Boissard, S. Fraga, S. Bieler, T. Ruckle, F. Vilbois, S. Robinson, M. Mutter, W. Banks and C. Soto, Pharmacological profiles of peptide drug candidates for the treatment of Alzheimer's disease, *J. Biol. Chem.*, 2003, **278**, 13905–13911.
- 49 D. Youngblood, S. Hatlevig, J. Hassinger, P. Iversen and H. Moulton, Stability of cell-penetrating peptide-



- morpholino oligomer conjugates in human serum and in cells, *Bioconjugate Chem.*, 2007, **18**, 50–60.
- 50 H. Chiang and J. Dice, Peptide sequences that target proteins for enhanced degradation during serum withdrawal, *J. Biol. Chem.*, 1988, **263**, 6797–6805.
  - 51 L. Tjernberg, C. Lilliehöök, D. Callaway, J. Näslund, S. Hahne, J. Thyberg, L. Terenius and C. Nordstedt, Controlling amyloid  $\beta$ -peptide fibril formation with protease-stable ligands, *J. Biol. Chem.*, 1997, **272**, 12601–12605.
  - 52 A. Roher, J. Lowenson, S. Clarke, C. Wolkow, R. Wang, R. Cotter, I. Reardon, H. Zürcher-Neely, R. Heinrikson and M. Ball, Structural alterations in the peptide backbone of beta-amyloid core protein may account for its deposition and stability in Alzheimer's disease, *J. Biol. Chem.*, 1993, **268**, 3072–3083.
  - 53 E. Luttmann and G. Fels, All-atom molecular dynamics studies of the full-length  $\beta$ -amyloid peptides, *Chem. Phys.*, 2006, **323**, 138–147.
  - 54 M. Wälti, F. Ravotti, H. Arai, C. Glabe, J. Wall, A. Böckmann, P. Güntert, B. Meier and R. Riek, Atomic-resolution structure of a disease-relevant  $A\beta_{(1-42)}$  amyloid fibril, *Proc. Natl. Acad. Sci. U. S. A.*, 2016, **113**, E4976–E4984.
  - 55 T. Lowe, A. Strzelec, L. Kiessling and R. Murphy, Structure–function relationships for inhibitors of  $\beta$ -amyloid toxicity containing the recognition sequence KLVFF, *Biochem.*, 2001, **40**, 7882–7889.
  - 56 M. Findeis, Peptide inhibitors of beta amyloid aggregation, *Curr. Top. Med. Chem.*, 2002, **2**, 417–423.
  - 57 Z. Chen, G. Krause and B. Reif, Structure and orientation of peptide inhibitors bound to beta-amyloid fibrils, *J. Mol. Biol.*, 2005, **354**, 760–776.
  - 58 H. Kundaikar and M. Degani, Insights into the interaction mechanism of ligands with  $A\beta_{42}$  based on molecular dynamics simulations and mechanics: implications of role of common binding site in drug design for Alzheimer's disease, *Chem. Biol. Drug Des.*, 2015, **86**, 805–812.
  - 59 S. Snyder, U. Lador, W. Wade, G. Wang, L. Barrett, E. Matayoshi, H. Huffaker, G. Krafft and T. Holzman, Amyloid-beta aggregation: selective inhibition of aggregation in mixtures of amyloid with different chain lengths, *Biophys. J.*, 1994, **67**, 1216–1228.

